All Theses and Dissertations

2015-12-01

Elucidating the Mechanisms of Rate-Dependent Deformation at Ambient Temperatures in a Model Metallic Glass

Matthew Bradley Harris
Brigham Young University

Elucidating the Mechanisms of Rate-Dependent Deformation

at Ambient Temperatures in a Model Metallic Glass

Matthew Bradley Harris

A thesis submitted to the faculty of
Brigham Young University
in partial fulfillment of the requirements for the degree of

Master of Science

Eric R. Homer, Chair
David T. Fullwood
Mike Miles

Department of Mechanical Engineering

Brigham Young University

December 2015

ABSTRACT

Elucidating the Mechanisms of Rate-Dependent Deformation
at Ambient Temperatures in a Model Metallic Glass

Matthew Bradley Harris
Department of Mechanical Engineering, BYU
Master of Science

In this work, the Shear Transformation Zone (STZ) dynamics model is adapted to capture the transitions between different regimes of flow serration in the deformation map of metallic glass. This was accomplished by scaling the STZ volume with a log-linear fit to the strain rate, and also adjusting the activation energy of an STZ with a log-linear fit to maintain constant yield strength at differing strain rates. Twelve simulations are run at each of six different strain rates ranging from 10^{-5} to 10^{0} s^{-1}, and statistics are collected on simulation behavior and shear band nucleation and propagation rates. The simulations show shear band nucleation has a positive correlation to strain rate, and shear band propagation has a negative correlation to strain rate. This shows that in STZ dynamics, the regime of reduced flow serration arises due to competing rates of nucleation and propagation, supporting the hypothesis proposed by Schuh. A positive correlation between critical shear band nucleus size and strain rate is proposed as an underlying cause of these rate dependencies.

ACKNOWLEDGEMENTS

TABLE OF CONTENTS

LIST OF TABLES

LIST OF FIGURES

1   INTRODUCTION

Metallic glasses show great promise as lightweight, high strength, flexible materials due to

their impressive mechanical properties [1-3]. However, metallic glasses suffer from poor

ductility at room temperature due to their tendency to localize plastic strain into shear bands [2,

4, 5], which ultimately lead to catastrophic failure. Interestingly, although the yield point of these

materials is not strain rate dependent, the shear band density and degree of flow serration depend

highly on strain rate [6, 7]. A thorough understanding of the mechanisms underlying this

phenomena would enable the development of tougher, more ductile metallic glass composites

and alloys.

The different modes of deformation, homogeneous and inhomogeneous, exhibited by

metallic glasses are well characterized by examination of Schuh's deformation map, shown in

Figure 1, adapted from [6]. The homogeneous regime exists at elevated temperatures and lower

strain rates, where the deformation is characterized by viscous flow. The inhomogeneous regime

is characterized by localized deformation in shear bands. This regime encompasses temperatures

below the glass transition temperature (T_g) at lower strain rates to a much larger temperature

range at higher strain rates. Within the inhomogeneous regime, deformation at low strain rates is

characterized by strongly serrated flow, meaning that strain accumulates in the material in

temporal bursts accompanied by relaxation stress drops resulting in a jagged stress-strain curve

[8, 9]. Higher strain rates are characterized by moderately serrated flow, and very high strain

1

rates have little or no flow serration. In nanoindentation experiments, Schuh and Jiang independently observed that this reduced flow serration was accompanied by a reduction in the appearance of shear steps in the surface of the material around the indenter [10, 11]. This indicates that plasticity in metallic glass is localized into only a few shear bands at lower strain rates, but allowed to disperse in to many shear bands at higher strain rates. It has been hypothesized that this change from few to many shear bands at increasing strain rate is due to competition between shear band nucleation and propagation; when individual shear bands nucleate and propagate quickly relative to the strain rate, the stress in the surrounding material is reduced, suppressing additional shear band nucleation. However, when shear bands do not accommodate strain quickly enough to relieve stress in the material, multiple shear bands occur to reduce the stress [7].
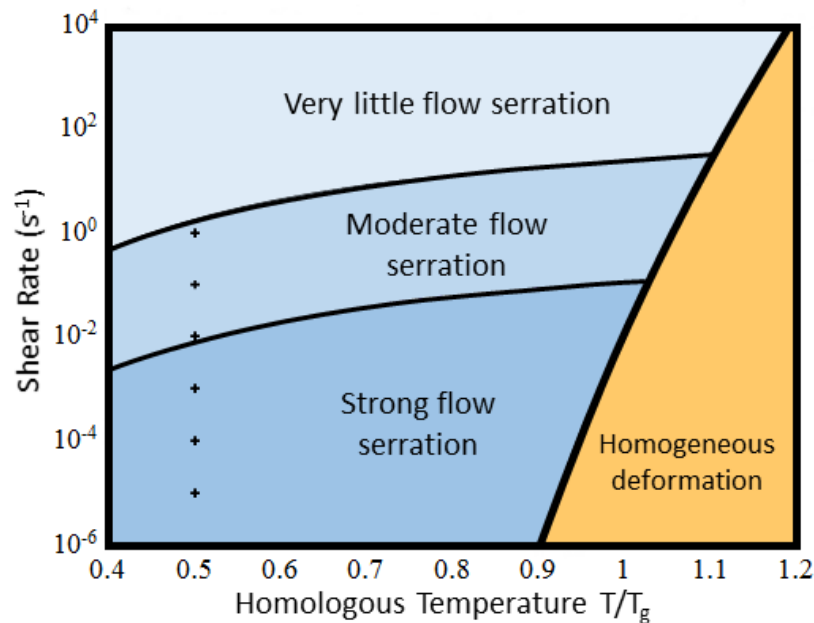

Figure 1: General Deformation Map of Metallic Glass
Deformation map scaled to the glass transition temperature (T$_g$) for a given glass, adapted from [6]. Points investigated in this paper are marked with a '+' on the deformation map.

The process by which individual shear bands nucleate, propagate, and arrest has been the subject of continued investigation. To understand this process, we begin with the fundamental unit of deformation in metallic glasses, which is accepted to conform to the shear transformation zone (STZ) theory introduced by Argon [12]. The STZ involves the collective and inelastic rearrangement of several dozen atoms in response to an applied shear stress. The action of one STZ causes an increase in the local stress field along the direction of shear, creating preferential sites for the activation of additional STZs [13, 14]. Models applying Argon's STZ theory have differed on how shear bands form and propagate from an initial group of STZs, with three main viewpoints being most prominent. First, some model the shear band as a percolating boundary that reaches a critical concentration before initiating simultaneous slip along the plane of highest resolved shear stress [15]. Second, shear bands are modeled as a propagating zone of rejuvenated glass, followed by a zone of glue-like material, and finally followed by liquid material, as adiabatic heating decreases the local strength [16]. Third, others model a two-step process, with a shear band nucleating from a small cluster of STZs, and propagating quickly through the sample before initiating simultaneous slip [17, 18]. Recent work by Qu, et al. has shown that metallic glass samples pulled to very low levels of plastic strain show signs of partially propagated shear bands [19], lending further credibility to the second and third theories. The two-step theory, as explained by Homer, Schuh, Greer and others [6, 14, 17, 18, 20], can be subdivided into three stages for the progression of deformation in metallic glasses:

1. Nucleation: STZs activate, cluster, and make up the growing nuclei of competing shear bands

2. Propagation: when a shear band nucleus reaches a critical size, it begins to rapidly grow, dominating plasticity in the region

3. Sliding: Stress relaxation occurs as the fully developed shear band thickens and accumulates additional plasticity as shear band slip, until the applied load decreases enough for slip to arrest

Once a shear band has arrested, the free volume generated by the action of STZs remains, and allows it to be preferentially reactivated [21-23]. Generally, in other works stages 1 and 2 are referred to as shear band initiation, while stage 3 is referred to as shear band propagation. In this paper, shear bands are analyzed for their progression through these stages. Stage 1, nucleation, ends when a shear band becomes dominant, stage 2, propagation, continues until the shear band reaches the full width of the simulation, and stage 3, sliding, encompasses all plasticity that takes place on the band after it is fully propagated.

Investigating the transition between different flow serration regimes requires a collection of shear band events to be studied in a statistical manner, so an understanding can be gained of how the mechanics of shear band formation influence flow serration. Researchers have used several different approaches to resolve shear band events in experimental setups. For example, high speed cameras have been able to capture shear band sliding, and measure shear band velocities [24]. They also show that flow serration is often the result of the same shear band being activated multiple times, rather than unique shear bands for each event [21]. Analysis of pop-in stresses during nanoindentation enabled estimation of STZ volumes and rate effects [25, 26]. Although this information is very useful, such experimental methods are unable to reveal the details of what is happening at the STZ level in shear band nucleation and propagation; the time and length scales of individual STZs are too small and fast for current measurement resolutions to capture directly, and indirect measurements do not give a complete picture.

Modeling techniques provide unique insight into the possible processes of shear band formation. Atomistic simulations do well at simulating the action of individual STZs, capturing the onset of shear localization in metallic glass [27]. They can measure the STZ volume for various glass compositions, and have shown that the instability of shear bands arises from

4

structural disordering in an STZ, rather than thermal softening [18, 28]. Constitutive models do well at recreating the macroscopic behavior of metallic glass. By treating the glass as a continuum material, rather than trying to simulate each individual atom or STZ, they enable more complicated structures and loads to be modeled, within the limits of the constitutive model's scope [29, 30]. Mesoscale models are needed to investigate the range of time and length scales intermediate to molecular dynamics and constitutive models [27]. One such mesoscale model is the STZ dynamics model developed by Homer and Schuh [31]. The STZ dynamics model is able to capture a broad range of time scales associated with shear band events in an efficient manner by using a kinetic Monte Carlo algorithm [13]. It has been used to simulate both 2D and 3D metallic glass structures; it predicts a propagating shear band, and captures the transition from inhomogeneous to homogeneous flow at the glass transition temperature [20, 32]. It has even been adapted by Li to account for free volume generation due to STZ activity [33]. Since this model is capable of simulating the nucleation and growth of multiple shear bands, and these are the parameters of interest, we use the STZ dynamics model for our investigation of flow serration regimes in metallic glasses.

In this work, the STZ dynamics model is adjusted to maintain a constant yield point at varying strain rates, consistent with metallic glass behavior. With the adjusted model parameters, we examine flow serration and shear band nucleation and propagation across a range of strain rates, with multiple simulations at each strain rate to establish statistical significance. Discussion of the results shows support for the hypothesis of competing shear band nucleation and propagation rates, and is focused on determining the underlying causes of this interaction. A hypothesis is developed to explain the simulated behaviors, and its implications are explored in the conclusion.

2   METHODS

2.1   STZ Dynamics Modeling Framework

The STZ dynamics model is built around the STZ as the fundamental unit of deformation in metallic glass. The STZs are coarse-grained by replacing groups of atoms with the features of a finite-element mesh. Each node in the mesh represents the center of a potential STZ, and the five to seven elements touching that node represent the atoms which collectively shear if that STZ is activated [31]. Each element can participate in different STZs, just as atoms may participate in various STZs in a real material. These course-grained STZs are treated mathematically as Eshelby inclusions with coherent boundaries, the same approach originally used by Argon, where the STZ is allowed to plastically deform as if in a vacuum and then forced elastically back into the surrounding matrix [12]. The kinetic Monte Carlo (kMC) algorithm is used to control the evolution of the modeling framework. When a given STZ is selected for shearing by the kMC algorithm, plastic strains are applied to the elements to simulate the simultaneous plastic shearing of atoms in the STZ. After each kMC step, finite-element analysis solves for the resulting stress and strain fields throughout the simulation, which then influence the selection of STZs in subsequent kMC steps [31].

The kMC algorithm works by listing all the possible transitions a system can make, calculating each transition's associated rate, and then using a random number to select one of the transitions for execution. Time in the simulation is then advanced by Δt based on the residence

time in the current configuration, which is also based on the rates of the possible transitions. A more complete description of the kMC algorithm is available from Voter [34]. In STZ dynamics, a modified kMC algorithm, introduced previously [13], is used to ensure that realistic times and transitions are represented. This is accomplished by suppressing any STZ events selected by the algorithm which would activate in a Δt greater than a certain maximum allowed time step, Δt_{max}. When this happens, the model increments time by Δt_{max} without activating any STZ. This allows other time-dependent parameters, such as stress and strain, to update on a reasonable time scale in a dynamic simulation beginning at very low stresses. After every time increment, whether an STZ is activated or not, finite element analysis (FEA) solves for the new stress distribution in the mesh, and new activation rates are calculated for use in the kMC algorithm.

The kMC algorithm requires a rate calculation for each possible event in its catalogue for selection. For the STZ dynamics framework, this is an STZ activation rate that calculates the rate at which a given STZ will transition form an unsheared to a sheared state. The activation rate $\dot{s}$ for shearing a particular STZ in one direction is given by:

$$\dot{s} = v_0 \exp\left(-\frac{\Delta F - \frac{1}{2}\tau\gamma_0\Omega_0}{kT}\right) \tag{1}$$

where v_0 is the attempt frequency (related to the Debye frequency), ΔF is the set activation energy barrier for shearing an STZ, T is the temperature in Kelvin, k is Boltzmann's constant, τ is the local shear stress in the direction of shear, γ_0 is the incremental shear strain applied to an STZ, and Ω_0 is the volume of an STZ. This rate captures the thermally activated nature of the shearing process, which can be biased by both its local shear stress, τ and the temperature, T. A more detailed explanation of this equation's parameters as they relate to the STZ dynamics model can be found in previous work [31].

The coarse-graining of the STZs follows previous works where node-centered STZs are defined on a uniquely generated, irregular, triangular mesh [31]. The mesh size is defined such that the average radius of the potential STZs is equal to the target STZ radius. Each simulation is generated with a length of 250 nm along the tensile axis, and a width of 50 nm. The long sides of the simulation are unconstrained, and the top and bottom surfaces of the simulation are allowed to move laterally relative to each other to enable lateral slip. The simulated tensile test is displacement controlled; this is achieved by constraining the bottom nodes, while the top nodes are displaced at a fixed velocity corresponding to the desired initial strain rate. In each step of the simulation, the nodes move in varying increments of strain corresponding to the elapsed time from the modified kMC algorithm.

The simulations are run at six different initial strain rates: 10^{-5}, 10^{-4}, 10^{-3}, 10^{-2}, 10^{-1}, and 10^{0} s^{-1}. With the simulation size of 250 nm, this results in displacement velocities that range from 0.0025 to 250 nm/s at the lowest and highest strain rates, respectively. Each simulation is run for as many kMC steps as necessary for the simulation to reach 1.9% total strain, regardless of strain rate. The maximum time step values for the modified KMC algorithm are set at 5, 1, 0.5, 0.05, 0.005, and 0.0005 seconds, increasing from the longest time at the lowest strain rate to the shortest time at the highest strain rate. This variation in Δt_{max} from one strain rate to the next is necessary to provide the needed time resolution that stabilizes the yield strength in each strain rate, balanced against a reasonable number of kMC steps for a given simulation. As an extreme example: at the 10^{0} s^{-1} strain rate, a large Δt_{max} like 1 s would cause 100% strain to be reached in the first kMC step, before any STZs are able to activate. On the opposite end, a small Δt_{max} such as .001 s used on the 10^{-5} s^{-1} strain rate, would require 10^{6} simulation steps to reach 1% strain, still short of yield. A representative strain rate was tested with several different values for

Δt_{max} spanning two orders of magnitude, and it is found that this parameter has no noticeable effect on yield strength or STZ behavior, other than to overshoot the yield strength when Δt_{max} is too large. Material property values used in the simulation correspond to those of Vitreloy 1, a commonly studied metallic glass, listed in Table 1; ΔF and Ω_0 are defined in the following section. The simulation temperature is held constant at 310 K, which is $0.5T_g$ for Vitreloy 1.

Table 1: Material Properties for Modeling Vitreloy 1
($Zr_{41.2}$ $Be_{22.5}$ $Ti_{13.8}$ $Cu_{12.5}$ Ni_{10})

Model Parameter	Name	Value
STZ strain	γ_0	0.1
Shear Modulus	μ_0	35.76 GPa [35]
Poisson's Ratio	ν	0.352 [35]
Debye Temperature	θ_D	327 K [36]

2.2 Parameterization of Strain Rate Dependence

The STZ dynamics model relies on the rate equation of STZ activation (Eq. 1) to control the evolution of the simulation and, as a result, it has an inherent strain rate dependence that leads to an increase in yield strengths. This is accompanied by increased shear band density at higher strain rates, which corresponds with the flow serration being studied. In order to capture the strain rate independence of yield strengths in metallic glasses [6] the STZ dynamics model is adjusted in this work. To modify the STZ dynamics model, we take inspiration from Dubach et al., who developed a constitutive model based on measurements of strain rate sensitivity and found that STZ volume has a log-linear relationship to strain rate at low temperatures [29]. Dubach's log-linear relationship of STZ volume has a positive correlation with strain rate (i.e. increased STZ volume at higher strains). However, when their strain-rate dependent function of

STZ volume is implemented in the STZ dynamics model, it intensifies the yield strength dependence on strain rate. Instead, we adopt the log-linear dependence of STZ volume with strain rate, but utilize a negative correlation (i.e. decreased STZ volume at higher strains). This follows the work of Tönnies et al., who measured nanoindentation pop-in stresses and found that the initiation of a shear band is increasingly confined to a more local activation volume at ambient temperature with increasing stress and loading rate [26]. While this at first appears to contradict the findings of Dubach et al., the results of the simulations given hereafter indicate agreement with Dubach's work, in that the critical shear band nucleus size increases with strain rate.

In examining the influence of different model parameters one can show that an STZ volume (Ω_0) and an activation energy (ΔF) that both decrease with increasing strain rate lessen the strain rate dependence of the yield strength while maintaining the increased shear band density at higher strain rates typical to metallic glasses. These are given by the following log-linear forms:

$$
\begin{aligned}
\Omega_0 &= -0.03772 \log_{10} \dot\epsilon + 1.6 \quad [nm^3] \\
\Delta F &= -0.0227405 \log_{10} \dot\epsilon + 1.07945 \quad [eV]
\end{aligned}
\tag{2}
$$

The STZ volume increases by 0.2 nm^3 for each order of magnitude change in strain rate, ranging from 2.6 to 1.6 nm^3, at the lowest and highest strain rates, respectively. These values are consistent with STZ volumes found generally [14, 37][20, 37], and the range of size found by Dubach et al. in their low temperature data [29]. The magnitude of ΔF across the strain rates ranges from 1.08 eV to 1.68 eV, which is also in line with expectations [let's talk about references here].

Figure 2 shows the results of the parameterization of strain rate dependence on the observed yield strength. Before fitting, there is a clear log-linear relationship between yield strength and strain rate, where a logarithmic fit has an R^2 value of 0.9625. After parameterizing Ω_0 and ΔF to strain rate, however, the R2 of the logarithmic fit of the yield strengths is reduced to 0.0271, meaning that the logarithmic fit of the yield strength no longer describes the relationship significantly better than the arithmetic mean; any variation is now ascribed to random noise in the data. Thus, the parameterization has been successful in eliminating the model's yield strength dependence on strain rate.
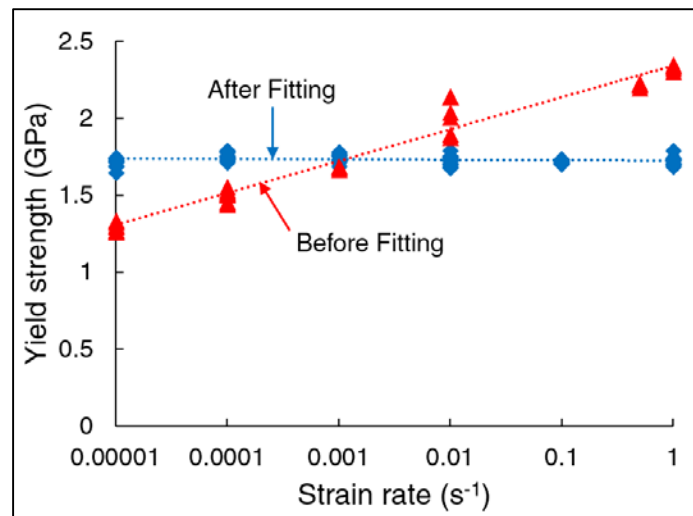

Figure 2: Yield Strength Dependence on Strain Rate
Yield strength dependence on strain rate before (red triangles) and after (blue diamonds) adjusting STZ volume and activation energy. After adjustment, the yield strength dependence on strain rate is statistically insignificant.

2.3   Statistical Analysis Approach

The goal of this work is to understand the mechanisms underlying the transitions between different regimes of flow serration in the deformation map. Emphasis is placed on measuring shear band nucleation and propagation rates since it is believed that different degrees of flow serration arise due to competition between these rates. In order to ensure statistical significance, twelve simulations are run at each of the six strain rates simulated, for a total of 72 simulations. At completion, the shear bands of each simulation are identified, as shown in Figures 3(a) and 3(b), where Figure 3(b) has each individual band highlighted in a unique color. These surrounding lines are placed carefully as they define which STZs contribute to each shear band, which is important for subsequent calculations. As a rule, any group of five or more STZs in a line is identified. Once the shear bands are identified, statistics are collected for:

1. The number of shear band nuclei in each simulation,
2. The dominance of individual shear bands during deformation,
3. Critical nucleus size of the first shear band when it becomes dominant,
4. Front propagation rate of each shear band,
5. Sliding velocity of the most dominant shear band once it has propagated across the entire simulation cell, and
6. The number and magnitude of stress drops in the simulation, which are used to measure the degree of flow serration in the simulation.

The manner in which each of these measurements is obtained is explained below, and demonstrated with an example simulation run at 10^{-4} s^{-1}, shown in Figure 3.

The number of shear band nuclei in each simulation is obtained by simply counting the number of shear bands identified, since each one must have started through the formation of a nucleus.
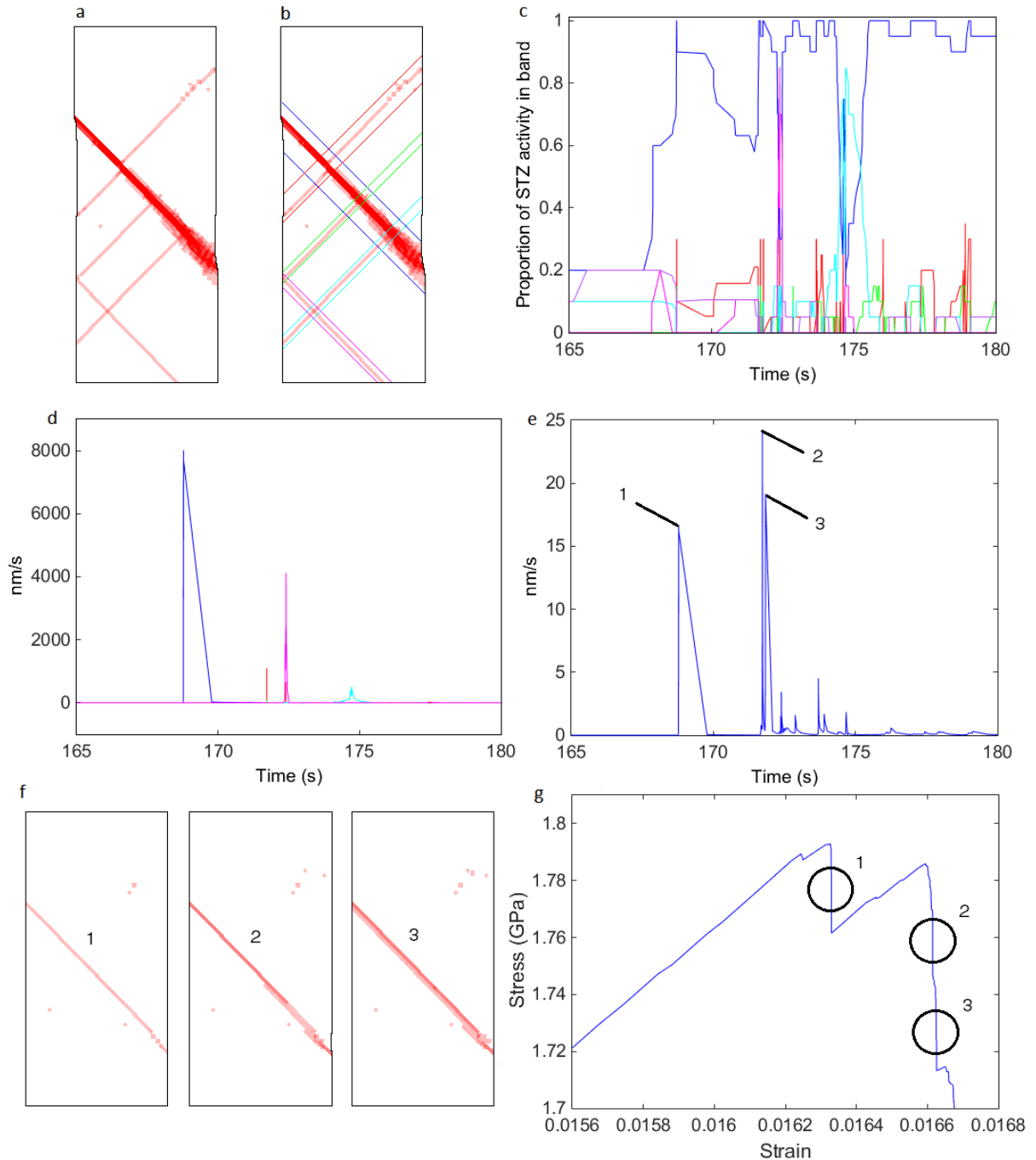
Figure 3: Methods Illustration of Measurements
(a) Partial raw simulation result. (b) Shear bands identified with surrounding lines of unique color. (c) Fraction of all STZ activity occurring in each shear band over time; unique colors match those in (b). (d) Propagation velocity of shear band front, corresponding to the unique color in (b). (e) Sliding velocity profile of the primary shear band, identified in blue in (b), with velocity bursts labeled 1, 2, and 3. (f) Snapshots of the simulation at time immediately following the bursts in (e) corresponding to labels 1, 2, and 3. (g) Stress drops on stress-strain curve corresponding to labels 1, 2, and 3 in (e), showing the stress drops resulting from sliding events on the active shear band.

The measurement of the critical nucleus size of a shear band requires knowledge of when an individual shear band has reached a critical size and accelerates its growth, thereby dominating deformation in that moment. As such, we introduce an additional measurement called shear band dominance, which is measured by examining a simulation using a moving window of twenty kMC steps. In each temporal window, the number of STZs activated in each shear band is totaled. Shear band dominance is defined as the fraction of STZs activated in a given shear band for that window in time. This window is moved in two kMC step increments to determine shear band dominance over the evolution of the whole simulation. This is plotted against time in Figure 3(c), with the colors in the plot matching the coloring of the shear band selection lines in Figure 3(b). A window can contain fewer than twenty activated STZs if some of the kMC steps do not produce STZ activations; this generally happens during the initial loading of the simulation, where the model is accumulating elastic strain. To prevent hypersensitivity to windows that contain very few STZ activations, no shear band can be dominant if that twenty kMC step window does not contain at least ten STZ activations. This has several implications; one is that when very few STZs are active, it is possible that the sum of STZ activity in the plot will amount to less than 100%. Similarly, some STZs in the simulation fall where two shear bands intersect; these STZs will count towards STZ activity in both shear bands and the sum of STZ activity can exceed 100%. Finally, even if all of the first twenty STZs in a simulation fall on the same shear band, the dominance ramps up to 100% rather than being instantly 100% dominant.

Shear band critical nucleus size is then defined as the total volume of STZs in a shear band nucleus at the point in time where it reaches a critical level of shear band dominance. A threshold of 60% dominance is chosen as the proportion of STZ activity required for a shear band to be

considered critical. In combination with the lower bound of ten STZs as the minimum number to be considered in calculating dominance, this means that the minimum critical shear band nucleus size that can be detected consists of six STZs. In this example simulation, the shear band marked with blue becomes dominant first, followed by the teal and magenta shear bands in later stages of the simulation. The shear bands marked with red and green never reach the threshold level of dominance. The critical nucleus sizes for each of these shear bands can be measured as their size when they become dominant, but for the purposes of this work, we examine only the first dominant shear band. This enables cleaner comparison in sizes between simulations and less variability in measurements due to shear band intersections later in the simulation.

Shear band propagation rate is measured by carefully finding the change in length of each shear band in a moving window of twenty kMC steps, then dividing that by the change in time for those twenty steps to give a velocity measurement. The evolution of the propagation speed is obtained by moving the window by two steps for each data point. The results of this measurement are plotted in Figure 3(d), with the same coloring scheme as in other parts of the figure.

Shear band sliding rate is defined as the relative velocity between the part of the mesh just above and just below the shear band. This is calculated by selecting several points on the shear band selection lines above and below a given shear band. The relative velocities of the nodes in the sliding direction is calculated using the same moving window used in previous calculations, and the results are given in Figure 3(e). Shear band sliding rate is measured only for the thickest, most dominant shear band in each simulation. This is done to reduce the amount of interference from shear band intersection and for clearer comparison between different simulations.

In order to measure flow serration, stress drops in each simulation are found by measuring the slope of the stress strain curve as shown in Figure 3(g). When the slope is large and negative, (a drop of at least 5 MPa in less than .000001 strain, for example) a stress drop is identified, with the value of the stress before and after the region of steep slope determining the magnitude of the drop as in [38]. Slopes are calculated in a moving window of twelve kMC steps, in order to prevent very small drops from dragging down average drop sizes. The average magnitude of these stress drops is used as a measure of flow serration in the simulation. It is noted that this approach differs from those generally used in experimental setups measuring flow serration, where flow serration is characterized by strain bursts. Furthermore, these stress drops do not have the appearance of serrated flow about a constant flow stress for a sample in compression [8]. However, the nanoscale size of the simulations do appear to match the general shape of the stress-strain response in experimental nanoscale tensile tests [39]. It is noted that the three stress drops in Figure 3(g) correspond to repeated activation of the same shear band, as shown by Figure 3(f).

3 RESULTS

Figure 4 (a) shows a group of six simulations, one from each strain rate studied, with increasing strain rate from left to right. The simulations shown represent typical results, with the number of shear bands in each one near the median value for its strain rate. Each simulation is shown at the final strain value of 1.9%. In general, low strain rates result in fewer, more dominant shear bands, with very few free STZs scattered outside the bands, while high strain rates feature larger numbers of less dominant shear bands, with many free STZs randomly scattered outside the bands. The stress strain curves for these six simulations are shown in Figure 4 (b), showing a tightly grouped yield strength around 1.72 GPa. While the yield strengths are similar, low strain rates tend to relax more quickly after yield, and have a lower flow stress than high strain rates.

3.1 Flow Serration

The average magnitude of stress drops in each simulation is measured as discussed in section 2.3. These average stress drops are then categorized and summarized by strain rate using box plots in Figure 5. These box plots mark the median value with the horizontal (red) line inside the box, the 1st and 3rd quartiles of the distribution bound the box, the extreme high and low values with whiskers that extend from the top and bottom of the box, and statistical outliers are marked as separate points. It can be seen that the average stress drop statistics have a negative
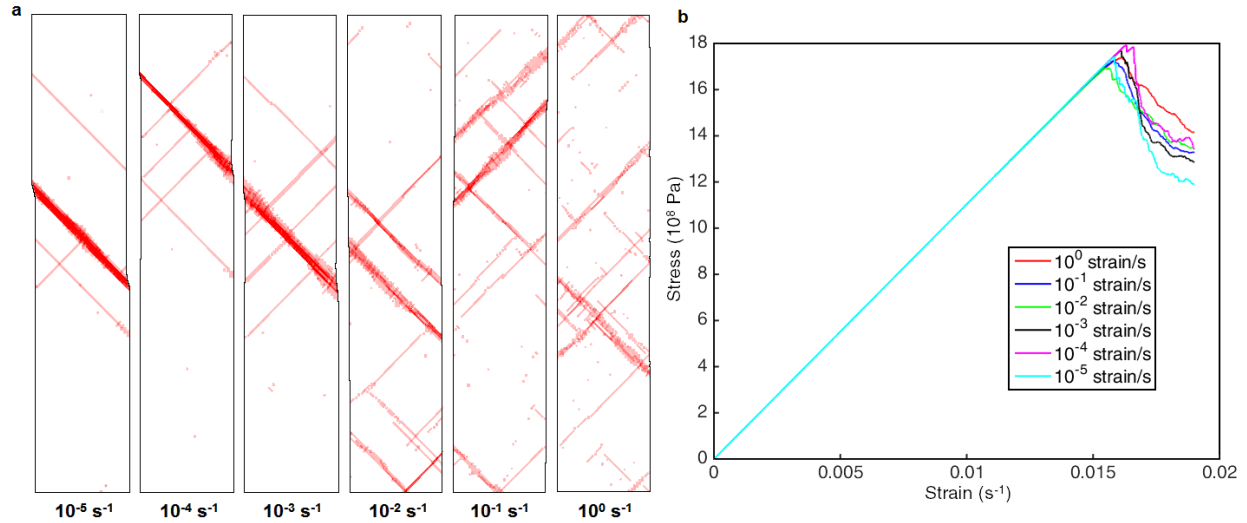
Figure 4: Results Overview
(a) Example simulation at each strain rate, where the number of shear bands in each simulation is near the median for that strain rate. Note the clear trend of increased shear band density with strain rate, and the increased appearance of free STZs in higher strain rates. (b) Stress-strain curves for the six simulations shown in (a).

correlation with strain rate. Strain rates in the Schuh's strong flow serration regime (lower strain rate to upper strain rate) have median values of 20-30 MPa, while those in the Schuh's moderate serration regime (upper and lower strain rate) have values of 7-15 MPa. There is a marked decrease at a strain rate of 10^{-2} strain/s, which is near the border of the transition from strong serration to light serration in Schuh's deformation map. The 10^{-2} strain rate also shows mixed behavior, with a few outlying simulations above the 20 MPa range. To understand how this change in flow serration is influenced by the mechanics of STZ activation, we now examine the statistics of shear band nucleation and propagation rates.

3.2 Shear Band Nucleation Statistics

Figure 6 provides statistics on the number of shear band nuclei, and the critical shear band nucleus size. Simulations at high strain rates show an increase in the number of shear band
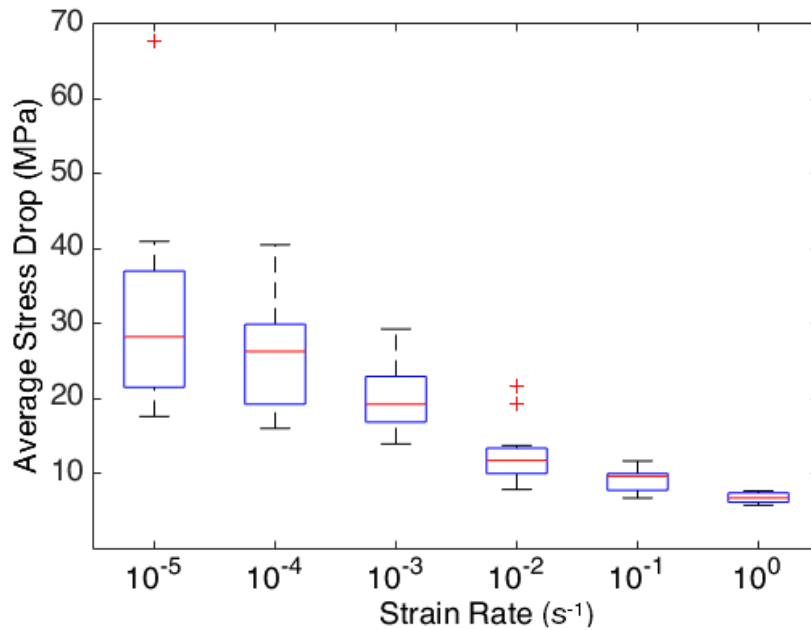
Figure 5: Average Stress Drop in Each Simulation by Strain Rate
A box plot of the average stress drop magnitude in each simulation, arranged by strain rate. This indicates decreased flow serration with increasing strain rate, matching the deformation map in Figure 1.

nuclei generated, as indicated by Figure 6(a). One can calculate the rate of shear band nucleation, in units of shear band nuclei generated per second, which is provided in the inset to Figure 6(a). However, the nucleation rate isn't necessarily the best comparison between different strain rates since the tests last different time periods. As such, the total number of nuclei (which is equivalent to nuclei per 1.9% strain), is the better comparison between strain rates. It is noted that the shear band nucleation rate has a positive correlation with strain rate. At low strain rates in the strong serration regime, a median of 4.5 to 6.5 shear band nuclei appeared throughout the entire simulation. At 10^{-2} s^{-1} and above this increases steadily, up to a median of 15.5 nuclei for the highest strain rate.

The statistics of the critical nucleus volume, or volume of the first shear band when it became dominant, is plotted in Figure 6(b). This critical volume has a positive correlation with strain rate. Something not captured in the plot is the fact that at the highest strain rate some of the simulations never have a shear band become dominant at all, resulting in fewer data points and an underestimation of the critical nucleus volume at that strain rate. Also, due to the fact that a lower bound is enforced on the measurement of critical shear band size, shear bands can never be considered dominant with fewer than six STZs. In Figure 6(b), we see that all strain rates from 10^{-5} to 10^{-2} s^{-1} have at least one simulation where the first shear band became dominant at exactly this lower bound. Thus, the lower bound may be overestimating the critical nucleus size for these slower strain rates. At the lowest strain rate, two or three STZs may be enough to reach a critical volume for the shear band to nucleate and propagate unconstrained.
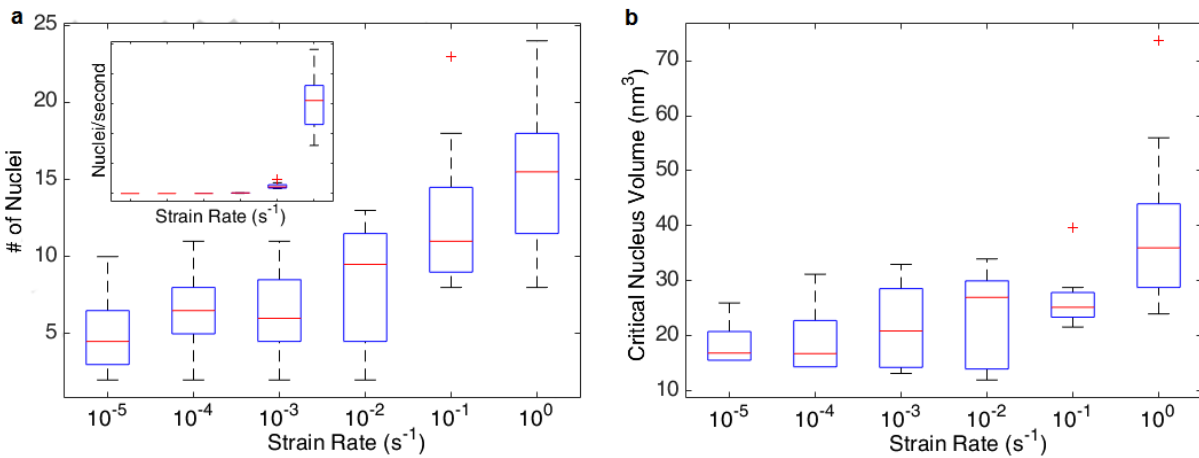
Figure 6: Nucleation Statistics
(a) Shows the nucleation rate after being normalized to strain rate. Inset shows the nucleation rate measured in shear band nuclei generated per second. The normalized rate shows a positive correlation between nucleation rate and strain rate. (b) Shear band critical nucleus size plotted against strain rate. The skew in lower strain rates is due to the cutoff size of detectable critical shear band nucleus size being reached.

3.3 Shear Band Propagation and Sliding Statistics

The statistics of the maximum propagation rate, or maximum speed of the shear band's propagating front, are presented as a rate, normalized by the strain rate in Figure 7(a). The unnormalized maximum propagating speed provided in the inset to Figure 7(a). Here it can be seen that before normalization, the maximum propagation speed of a growing shear band in a simulation at first seems to increase proportionally with the strain rate. However, the normalization indicates that at higher strain rates, the relative maximum propagation rate actually decreases with increasing strain rate. This means that while a single shear band grows faster at increasing strain rates, it is moving slower relative to the applied strain rate as that strain rate increases.
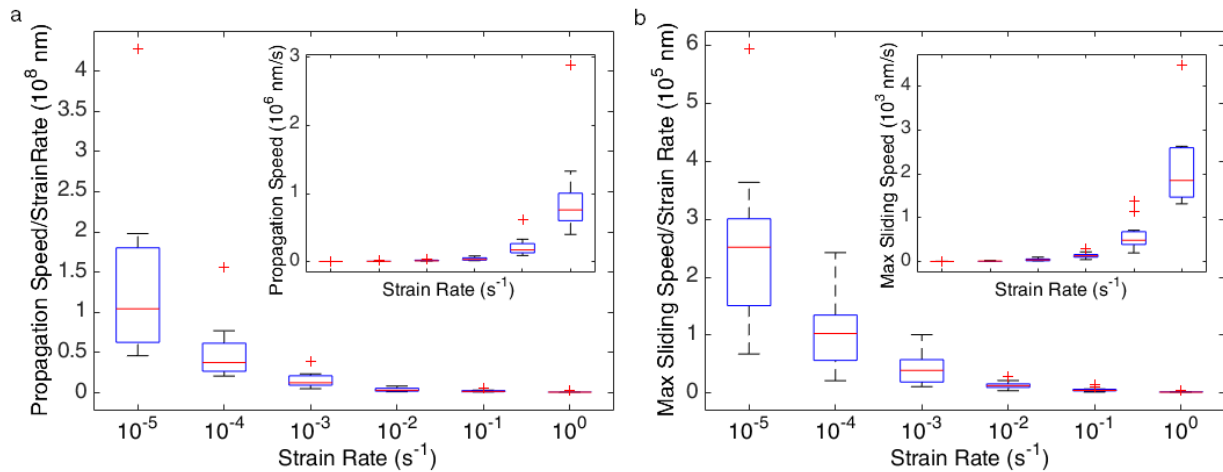
Figure 7: Propagation and Sliding Rate Statistics
(a) Maximum shear band propagation speed for each simulation. Inset is before normalizing to strain rate, main body shows after. (b) Maximum shear band sliding speed for each simulation. Inset is before normalizing to strain rate, main body shows after.

A similar relationship is found when looking at the maximum shear band sliding speed, which is shown in its strain rate normalized form in Figure 7(b). The unnormalized sliding speed

is provided as an inset to Figure 7(b). Once again, the unnormalized form goes from a positive correlation with strain rate to a negative correlation when it is normalized by the strain rate. This means that continued sliding of the largest shear band accounts for less and less of the total plasticity as the strain rate increases. By comparing Figure 7(a) to Figure 7(b), we also see that the normalized shear band propagation speed is about three orders of magnitude faster than the normalized shear band sliding speed, which is consistent with measurements related to the two-step shear band formation model, which place shear band propagation on the microsecond time scale and shear band sliding on the millisecond time scale [9].

In order to see how strain accumulates on the largest shear band over time, the shear band sliding speed is plotted against time for each simulation. Representatives of the highest and lowest strain rates are shown in Figure 8, with each plot appearing next to its respective simulation result. These simulations are chosen because each has a thick, dominant shear band, though these were rare at the highest strain rate. The graphs show that at the lowest strain rate, the dominant shear band accumulates plasticity in very sharp temporal bursts, with very little activity on the band in between these strain bursts. At the highest strain rate, even when the plasticity is concentrated mostly into a single band, the band accumulates plasticity in a more continuous manner, with less pronounced temporal bursts. This is illustrative of the flow serrations expected for the two strain rates, indicating that the model is producing the expected behaviors.
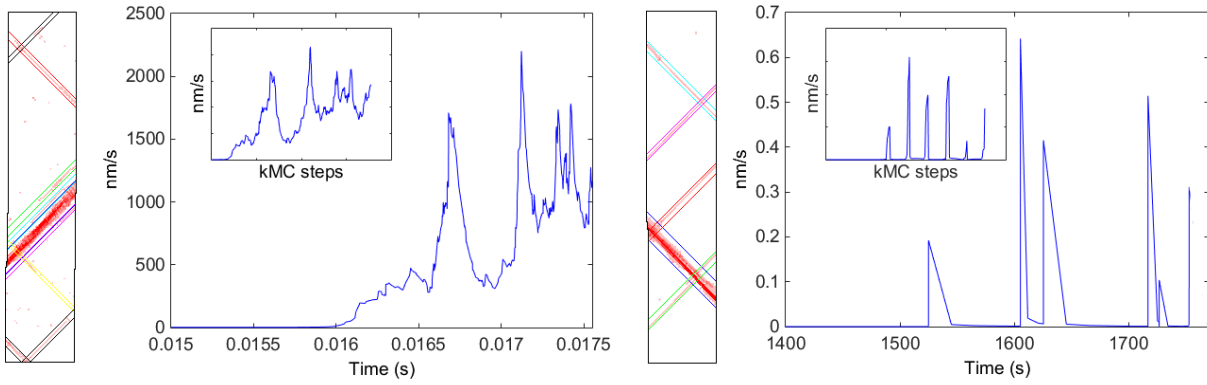
**Figure 8: Comparison of Shear Band Sliding at High and Low Strain Rates**
An example simulation from the fastest strain rate (left) and the slowest strain rate (right)
demonstrating that strain accumulated on the most dominant band in the simulation
continuously in the high strain rate, and in bursts at the low strain rate. Most simulations
at the highest strain rate did not have a dominant band this pronounced.

4 DISCUSSION

One important attribute of the STZ dynamics model is that the stochastic approach enables variation in a given process to be studied from identical starting simulation parameters. This variability partially fulfills Greer's suggestions for treating STZ behavior by statistical means, which he suggests due to the variance in STZ volumes and activation energy barriers measured in various atomistic models and experimental methods [14]. In Figure 5, for example, at 10-2 strain/s most simulations belong in the regime of moderate flow serration, while a few outliers seem to belong in the strong flow serration regime [7]. Similarly, in Figure 6(b), some of the simulations at 100 strain/s never ended up nucleating a dominant shear band, which can mean that they match Schuh's transition from light, to little or no flow serration in the deformation map [7]. Such variability near regime changes in the deformation map, where a given sample could exhibit behavior from either regime, could be expected in experimental results. This creates additional confidence that the model is capturing transitions between distinct regimes, rather than simply modeling a general trend of decreasing flow serration with increasing strain rate.

A summary of the different statistics and their strain rate dependence is shown in Figure 9, where each rate has been scaled so they can be compared side by side. This shows a transition from shear band propagation-driven plasticity that dominates at low strain rates, to shear band nucleation-driven plasticity that dominates at high strain rates. This shows strong support for the

24

hypothesis Schuh proposed, that the decreased flow serration seen at higher strain rates is due to the nucleation of many small shear bands in direct competition to the propagation of individual bands [10]. However, the underlying cause for this transition is not clear. One could question whether propagation is limiting nucleation, or vice versa. We hypothesize that the critical shear band nucleus size is an underlying cause of these rate dependencies. A shear band cannot begin to dominate the simulation until the critical shear band nucleus size is reached; if the critical shear band nucleus size increases, it will be harder for that size to be reached, which will encourage the growth of additional shear band nuclei. Similarly, if the critical shear band nucleus size is small, then shear bands become dominant very quickly, relaxing the stress, and preventing new shear band nuclei from forming. At the highest strain rate, the critical nucleus size is so large that some simulations fail to generate a dominant band at all, indicating that the critical nucleus size is larger than the simulated sample size.

The hypothesis of critical shear band nucleus size dependence on strain rate helps to reconcile our results with Dubach's constitutive model for the STZ volume. In section 2.3, Dubach's constitutive model is used to justify STZ volume having a log-linear dependence on strain rate, but it is noted that their log-linear dependence was positive, while ours is negative. Also, their linear dependence was at 77 K, while our simulations are running at 310 K. Dubach did not show a log-linear relationship between STZ volume and strain rate at ambient temperatures, but did show that much larger STZ volume were predicted, up to two orders of magnitude, and with a great deal more variability. Our critical shear band nucleus sizes more closely match the values Dubach found for that temperature than do our chosen STZ volumes, and the critical shear band nucleus size has a positive relationship with strain rate, matching Dubach's constitutive law. It could be that the acoustic emission data from which they calculated
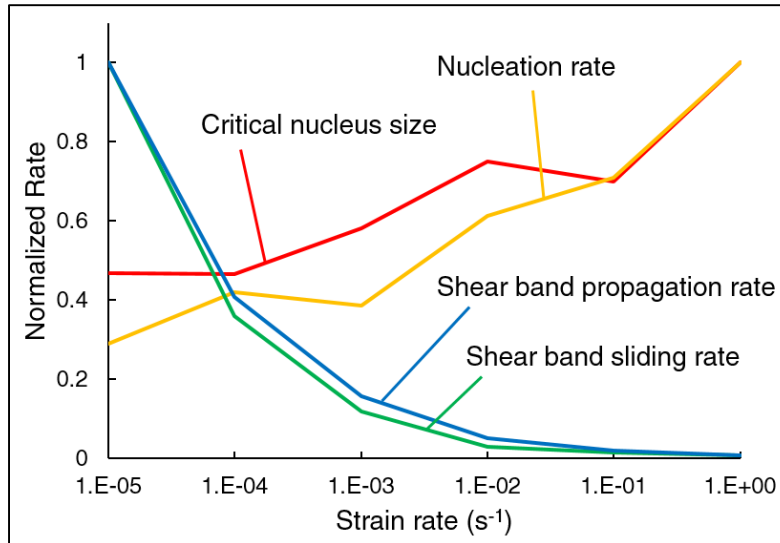
Figure 9: Comparison of Rates Measured
STZ dynamics confirms that competition between shear band nucleation rate, (yellow) and shear band propagation and growth rate (blue and green, respectively) is the likely cause of the transition of flow serration in the deformation map. Changes in the critical nucleus size (red) is a likely underlying cause. Recall that critical nucleus sizes for the lowest strain rates are slightly exaggerated due to the cutoff value in measuring them.

STZ volumes actually correspond to a critical nucleus size of the shear band, in which case the results of this work are reconciled with Dubach's at the simulated temperatures.

The results of this study can be summarized in terms of the stages of shear band development. At all strain rates, the sample deforms elastically before STZ activity begins. In stage 1, STZs appear, and begin to cluster into shear band nuclei, which grow and proliferate in the absence of a dominant shear band. If the strain rate is low, then a small critical nucleus size means that stage 2 is reached quickly, and one shear band rapidly propagates across the sample, and begins to dominate all plasticity in the sample. Then, in stage 3, additional plasticity is concentrated in bursts on that dominant band. If instead the strain rate is high, then a large critical nucleus size means that stage 2 is delayed, or skipped entirely, and plasticity continues to be accommodated by nucleation of additional shear band nuclei in stage 1. Then sliding in stage

3 occurs more gradually as shear band nuclei begin to intersect each other, and plasticity remains relatively diffuse.

Speculating that critical shear band nucleus size is indeed the controlling factor indicates that the parameterization of STZ volume and STZ energy barrier as a function of strain rate may capture physical mechanisms of STZs. Experiments do indicate a STZ size dependence on strain rate [26, 29], but STZ volume and energy barrier dependence in this model could also be surrogates for some other behavior. For example, an effective change in volume or a change in energy barrier could actually be the result of free volume redistribution. For example, the STZ may have an effectively larger size or larger energy barrier at lower strain rates because it has more time for free volume redistribution to extract the low energy events so only the larger transition barriers remain [40, 41]. Alternatively, one could ascribe the change to some other phenomena like local elastic properties [42] or local bonding such as icosahedral or non-icosahedral effects [43]. In any case, it is noted that the variation of the energy barrier (1.08-1.68 eV) and the STZ volume (1.6-2.6 nm3) is small and has log-linear dependence. These variations are likely within the resolution of techniques used to measure them. This functional dependence of these values may also explain the variation in reported measurements since different rates will result in different values. In the end, the experiments and the present simulations both indicate a rate dependence to the STZ behavior, which changes the critical nucleus size for shear banding. These minor changes lead to substantially different shear banding behaviors over the range of strain rates studied.

Finally, the critical nucleus size also has implications for improving ductility in metallic glasses. It is known that annealing/quenching and mechanical deformation can influence the ductility [44], perhaps these can be used to influence the glass and increase the number of

nucleation sites to the point that the glass is forced to deform in a more homogeneous manner. In addition, critical shear band nucleus size may also help explain why metallic glasses exhibit size-dependence for small samples. Metallic glass samples which are less than one mm in width are able to deform plastically more readily than larger samples; this is true for tension, compression, and bending [45-48]. Just as in the highest strain rate, where some shear bands traversed the shear band before achieving the critical nucleus size, perhaps the smaller experimental samples nucleate lots of shear bands because not enough dominant shear bands are nucleated.

5 CONCLUSION

This study shows that the changes in the degree of flow serration with strain rate on the general deformation map of metallic glass can be modeled accurately using STZ dynamics. Running twelve replicate simulations at each of six strain rates ranging from 10^{-5} to 10^{0} s^{-1}, allows statistical data to be gathered about the simulations: measuring shear band nucleation rate and flow serration. It also allows statistical data to be gathered about the behavior of individual shear bands: measuring critical shear band nucleus size, propagation rates, and sliding rates. This results in identifying clear correlations between nucleation or propagation statistics and strain rate, which also correspond to the changes in flow serration regimes. The nucleation rate, measured in nuclei generated for a given strain, shows a positive correlation to strain rate, with the highest rate generating a median number of shear band nuclei more than three times that of the lowest strain rate. Shear band propagation and sliding rates, measured in nm/strain, show a negative correlation to strain rate. These measurements combined show support for Schuh's hypothesis that the flow serration regimes arise from competing nucleation and propagation rates. A new hypothesis is proposed that these rate dependencies arise from an underlying positive rate dependence on critical shear band nucleus size, which is controlled in STZ dynamics by modifying the STZ volume and STZ energy barrier. Free volume generated by STZs may also affect the critical shear band nucleus size at different strain rates, but is not included in this study. If the critical shear band nucleus size is the underlying cause of rate

29

dependent deformation, this could be exploited to allow room temperature ductility in bulk metallic glasses. This could happen by adjusting metallic glass composition, heat treating by annealing or quenching, or by fine-tuning the spacing between dendrites in metallic glass matrix composites. In order to test this new hypothesis, more accurate experimental and modeled measurements of STZ volume, STZ energy barrier, and critical shear band nucleus size are needed.

REFERENCES

1. Telford, M., *The case for bulk metallic glass.* Materials Today, 2004. **7**(3): p. 36-43.

2. Wang, W.H., C. Dong, and C.H. Shek, *Bulk metallic glasses.* Materials Science and Engineering: R: Reports, 2004. **44**(2–3): p. 45-89.

3. Homer, E.R., et al., *New Methods for Developing and Manufacturing Compliant Mechanisms Utilizing Bulk Metallic Glass.* Advanced Engineering Materials, 2014. **16**(7): p. 850-856.

4. Ashby, M.F. and A.L. Greer, *Metallic glasses as structural materials.* Scripta Materialia, 2006. **54**(3): p. 321-326.

5. Pampillo, C., *Flow and fracture in amorphous alloys.* Journal of Materials Science, 1975. **10**(7): p. 1194-1227.

6. Schuh, C.A., T.C. Hufnagel, and U. Ramamurty, *Mechanical behavior of amorphous alloys.* Acta Materialia, 2007. **55**(12): p. 4067-4109.

7. Schuh, C.A., A.C. Lund, and T.G. Nieh, *New regime of homogeneous flow in the deformation map of metallic glasses: elevated temperature nanoindentation experiments and mechanistic modeling.* Acta Materialia, 2004. **52**(20): p. 5879-5891.

8. Song, S.X., et al., *Flow serration in a Zr-based bulk metallic glass in compression at low strain rates.* Intermetallics, 2008. **16**(6): p. 813-818.

9. Dalla Torre, F.H., et al., *Stick–slip behavior of serrated flow during inhomogeneous deformation of bulk metallic glasses.* Acta Materialia, 2010. **58**(10): p. 3742-3750.

10. Schuh, C.A., et al., *The transition from localized to homogeneous plasticity during nanoindentation of an amorphous metal.* Philosophical Magazine, 2003. **83**(22): p. 2585-2597.

11. Jiang, W.H. and M. Atzmon, *Rate dependence of serrated flow in a metallic glass.* Journal of Materials Research, 2003. **18**(4): p. 755-757.

12. Argon, A.S., *Plastic deformation in metallic glasses.* Acta Metallurgica, 1979. **27**(1): p. 47-58.

13.   Homer, E.R., D. Rodney, and C.A. Schuh, *Kinetic Monte Carlo study of activated states and correlated shear-transformation-zone activity during the deformation of an amorphous metal.* Physical Review B, 2010. **81**(6): p. 064204.

14.   Greer, A.L., Y.Q. Cheng, and E. Ma, *Shear bands in metallic glasses.* Materials Science and Engineering: R: Reports, 2013. **74**(4): p. 71-132.

15.   Ogata, S., et al., *Atomistic simulation of shear localization in Cu–Zr bulk metallic glass.* Intermetallics, 2006. **14**(8–9): p. 1033-1037.

16.   Shimizu, F., S. Ogata, and J. Li, *Yield point of metallic glass.* Acta Materialia, 2006. **54**(16): p. 4293-4298.

17.   Klaumünzer, D., R. Maaß, and J.F. Löffler, *Stick-slip dynamics and recent insights into shear banding in metallic glasses.* Journal of Materials Research, 2011. **26**(12): p. 1453-1463.

18.   Cao, A.J., Y.Q. Cheng, and E. Ma, *Structural processes that initiate shear localization in metallic glass.* Acta Materialia, 2009. **57**(17): p. 5146-5155.

19.   Qu, R.T., et al., *Progressive shear band propagation in metallic glasses under compression.* Acta Materialia, 2015. **91**(0): p. 19-33.

20.   Homer, E.R., *Examining the initial stages of shear localization in amorphous metals.* Acta Materialia, 2014. **63**(0): p. 44-53.

21.   Song, S.X. and T.G. Nieh, *Direct measurements of shear band propagation in metallic glasses – An overview.* Intermetallics, 2011. **19**(12): p. 1968-1977.

22.   Wright, W.J., T.C. Hufnagel, and W.D. Nix, *Free volume coalescence and void formation in shear bands in metallic glass.* Journal of Applied Physics, 2003. **93**(3): p. 1432-1437.

23.   Kanungo, B.P., et al., *Characterization of free volume changes associated with shear band formation in Zr- and Cu-based bulk metallic glasses.* Intermetallics, 2004. **12**(10–11): p. 1073-1080.

24.   Song, S.X., X.L. Wang, and T.G. Nieh, *Capturing shear band propagation in a Zr-based metallic glass using a high-speed camera.* Scripta Materialia, 2010. **62**(11): p. 847-850.

25.   Choi, I.-C., et al., *Estimation of the shear transformation zone size in a bulk metallic glass through statistical analysis of the first pop-in stresses during spherical nanoindentation.* Scripta Materialia, 2012. **66**(11): p. 923-926.

26.   Tönnies, D., et al., *Rate-dependent shear-band initiation in a metallic glass.* Applied Physics Letters, 2015. **106**(17): p. 171907.

27. Rodney, D., A. Tanguy, and D. Vandembroucq, *Modeling the mechanics of amorphous solids at different length scale and time scale.* Modelling and Simulation in Materials Science and Engineering, 2011. **19**(8): p. 083001.

28. Zink, M., et al., *Plastic deformation of metallic glasses: Size of shear transformation zones from molecular dynamics simulations.* Physical Review B, 2006. **73**(17): p. 172203.

29. Dubach, A., F.H. Dalla Torre, and J.F. Löffler, *Constitutive model for inhomogeneous flow in bulk metallic glasses.* Acta Materialia, 2009. **57**(3): p. 881-892.

30. Anand, L. and C. Su, *A constitutive theory for metallic glasses at high homologous temperatures.* Acta Materialia, 2007. **55**(11): p. 3735-3747.

31. Homer, E.R. and C.A. Schuh, *Mesoscale modeling of amorphous metals by shear transformation zone dynamics.* Acta Materialia, 2009. **57**(9): p. 2823-2833.

32. Homer, E.R. and C.A. Schuh, *Three-dimensional shear transformation zone dynamics model for amorphous metals.* Modelling and Simulation in Materials Science and Engineering, 2010. **18**(6): p. 065009.

33. Li, L., E.R. Homer, and C.A. Schuh, *Shear transformation zone dynamics model for metallic glasses incorporating free volume as a state variable.* Acta Materialia, 2013. **61**(9): p. 3347-3359.

34. Voter, A.F., *Introduction to the kinetic Monte Carlo method*, in *Radiation Effects in Solids*. 2007, Springer. p. 1-23.

35. Johnson, W.L. and K. Samwer, *A universal criterion for plastic yielding of metallic glasses with a (T/Tg) 2/3 temperature dependence.* Phys Rev Lett, 2005. **95**(19): p. 195501.

36. Wang, Q., et al., *Mechanical properties over the glass transition of Zr41.2Ti13.8Cu12.5Ni10Be22.5 bulk metallic glass.* Journal of Non-Crystalline Solids, 2005. **351**(27–29): p. 2224-2231.

37. Fu, X.L., Y. Li, and C.A. Schuh, *Homogeneous flow of bulk metallic glass composites with a high volume fraction of reinforcement.* Journal of Materials Research, 2007. **22**(06): p. 1564-1573.

38. Kimura, H. and T. Masumoto, *A model of the mechanics of serrated flow in an amorphous alloy.* Acta Metallurgica, 1983. **31**(2): p. 231-240.

39. Jang, D. and J.R. Greer, *Transition from a strong-yet-brittle to a stronger-and-ductile state by size reduction of metallic glasses.* Nat Mater, 2010. **9**(3): p. 215-219.

40. Rodney, D. and C. Schuh, *Distribution of Thermally Activated Plastic Events in a Flowing Glass.* Physical Review Letters, 2009. **102**(23): p. 235503.

41.   Delogu, F., *Thermal and mechanical activation of inelastic events in metallic glasses.* Scripta Materialia, 2016. **113**: p. 145-149.

42.   Tsamados, M., et al., *Local elasticity map and plasticity in a model Lennard-Jones glass.* Physical Review E, 2009. **80**(2): p. 026112.

43.   Egami, T., *Atomic level stresses.* Progress in Materials Science, 2011. **56**(6): p. 637-653.

44.   Jiang, W.H. and M. Atzmon, *Room-temperature flow in a metallic glass - Strain-rate dependence of shear-band behavior.* Journal of Alloys and Compounds, 2011. **509**(27): p. 7395-7399.

45.   Conner, R.D., et al., *Shear band spacing under bending of Zr-based metallic glass plates.* Acta Materialia, 2004. **52**(8): p. 2429-2434.

46.   Guo, H., et al., *Tensile ductility and necking of metallic glass.* Nat Mater, 2007. **6**(10): p. 735-739.

47.   Huang, J.C., J.P. Chu, and J.S.C. Jang, *Recent progress in metallic glasses in Taiwan.* Intermetallics, 2009. **17**(12): p. 973-987.

48.   Kumar, G., A. Desai, and J. Schroers, *Bulk Metallic Glass: The Smaller the Better.* Advanced Materials, 2011. **23**(4): p. 461-476.